

Spatial and Temporal Variation Characteristics of Nitrogen and Phosphorus in the Mudong River Basin of Karst Wetlands in Southwest China

Han Runhan¹, Pan Linyan^{2,3*}, Dai Junfeng^{1, 4*}, Huang Kai⁵, Du Ming¹, Hu Songli¹, Zeng Derong¹

¹ College of Environmental Science and Engineering, Guilin University of Technology, Guilin 541004, Guangxi, China

² College of Environment and Resources, Guangxi Normal University, Guilin 541004, China

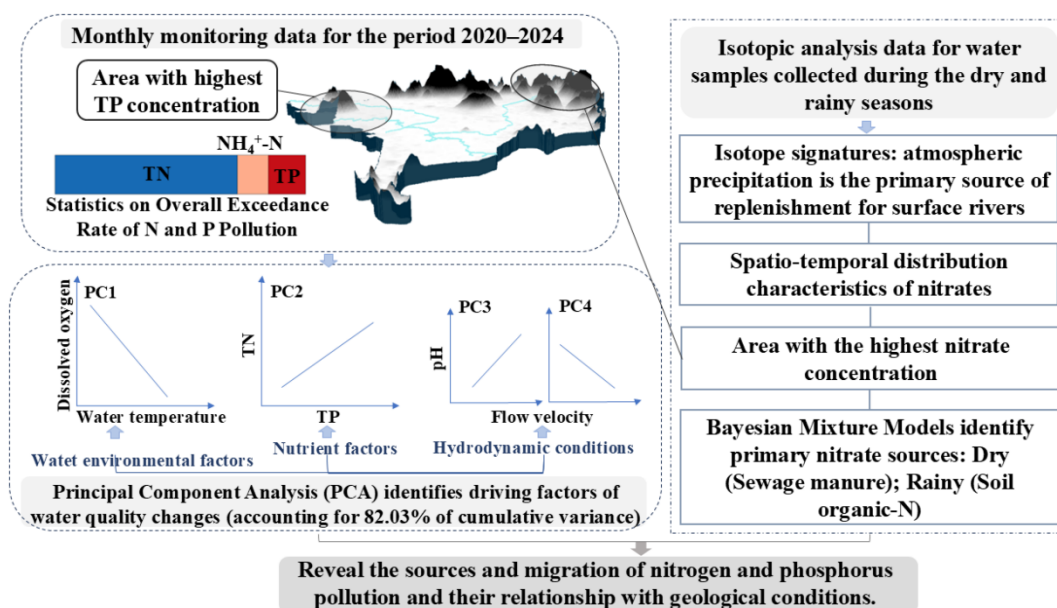
³ Guangxi Key Laboratory of Environmental Processes and Remediation in Ecologically Fragile Regions, Guilin China

⁴ Guangxi Key Laboratory of Environmental Pollution Control Theory and Technology, Guilin China

⁵ Guangxi Institute of Water Resources Research, Nanning China

* Corresponding author, e-mail: ann-fred@163.com; whudjf@163.com

Graphical abstract:



Abstract: The purpose of this study was to analyze the spatiotemporal distribution characteristics and driving factors of nitrogen (N) and phosphorus (P) in surface water of the Mudong River basin in Guilin, through hydrological monitoring, PCA (principal component analysis), and dual isotope tracing of nitrate. The results suggest that (1) Monitoring data show that total nitrogen (TN) is the main pollutant with seasonal variations. The exceedance rate reached a staggering 70.6%. The concentration is usually higher in the dry season. The concentrations of total phosphorus (TP) show a clear spatial, increasing trend from the upstream towards the downstream, with peak concentrations located at the western discharge. (2) As seen in the PCA results, water environmental factors (water temperature and dissolved oxygen), nutrient factors (TN and TP), and hydrodynamic conditions were the three input factors. (3) The Bayesian mixing model revealed a clear seasonal pattern in nitrate sources with a contribution from sewage manure as the major source during the dry season (37.9%) whereas it turned to soil organic-N in the rainy season (63.1%).

Key words: Nitrogen; Phosphorus; Isotopes; Source Apportionment; Karst

14 **1 Introduction**

15 The “kidney” of the earth, wetlands conserve species, the climate and purify water. Nevertheless,
16 human activity threatens wetland ecosystems more than ever and pollution by nitrogen (N) and
17 phosphorus (P) have become a global issue. Excessive nutrients N and P are essential, but they can
18 cause serious consequences such as water eutrophication, algal bloom, ecosystem imbalances
19 (Vitousek et al., 1997; Smith et al., 1999; Xue et al., 2009; Xu et al., 2020). In semi-arid zones and
20 regions with high agricultural activity, this phenomenon has pronounced effects (Liang et al., 2021;
21 Pan et al., 2021).

22 Nutrient pollution is especially serious in karst areas due to the geology of the region. As precipitation
23 and surface runoff infiltrate underground through cracks and other pathways, attenuation of the
24 nutrients is less (Reimann et al., 2011). Because of this direct pathway, farm and domestic pollutants,
25 such as fertilizer and manure, can rapidly move into groundwater and surface water with little
26 attenuation (Crain, 2010). The karst landscapes in Southwest China, for example, already underwent
27 severe nitrogen loss (Song et al., 2017). Moreover, these dissolution channels can also reduce the
28 hydraulic retention time of pollutants, thus weakening denitrification, organic matter degradation and
29 the like (Heffernan et al., 2012). The way of N and P migration and transformation in karst basins is
30 quite different from non-karst basins because of the unique geohydrological traits of these basins.
31 There is a shortage of studies that centre on relevant research.

32 At present, water pollution source tracing is being done by researchers the world over using stable
33 isotope techniques. The use of stable isotope analysis combined with hydrochemical data and mixing
34 models (SIAR/MixSIAR) has become an essential tool for tracing nitrogen sources and identifying

transformation processes. In a typical karst wetland in Guilin, China, Li et al. (2022) carried out a study, where they measured $\delta D-H_2O$, $\delta^{18}O-H_2O$, $\delta^{15}N-NO_3^-$, and $\delta^{18}O-NO_3^-$ in conjunction with the MixSIAR model. Their work quantitatively apportioned nitrate contributions from chemical fertilizers (33.4%), livestock and domestic wastewater (39.8%), and soil organic nitrogen (26.8%), thereby revealing the quantitative structure of nitrogen sources in the karst area (Li et al., 2022). Similarly, Guo et al. (2023), by integrating isotopic data with conventional hydrochemical ions and model analysis, effectively differentiated mixed pollution sources and concluded that nitrate pollution in the studied urban river was primarily derived from domestic wastewater and the nitrification of chemical fertilizers. Multi-isotope-based source analysis of nitrate nitrogen has also been carried out in the typical Huixian Karst Wetland of Guilin, Guangxi. Studies have indicated that artificial NH_4^+ fertilizers, soil nitrogen, and manure/sewage are the dominant sources of NO_3^- in this wetland (Liao et al., 2022). However, most existing research has focused on core wetland or groundwater zones, or has been limited by short monitoring periods. Significant gaps remain in understanding coupled basin-scale dynamics, seasonal variations between dry and rainy periods, the co-behavior of nitrogen and phosphorus, and the integrated analysis of karst hydrodynamics with isotopic tracers. Based on the aforementioned background, this study, conducted at a typical karst wetland watershed scale, aims to: (1) incorporate monitoring across both dry and rainy seasons to elucidate the spatiotemporal variations in nitrogen and phosphorus concentrations and identify their primary influencing factors; and (2) apply stable isotope techniques to identify pollution sources and, by integrating seasonal variations, reveal shifts in the contributions of different sources between dry and rainy periods, thereby enriching the perspective on seasonal dynamics of non-point source pollution

56 in karst regions.

57 **2 Materials methods**

58 **2.1 Study area**

59 The Mudong River Basin is located in Lingui District, Guilin City, Guangxi Zhuang Autonomous
60 Region, China, and belongs to the irrigation area governed by the West Main Drainage Channel of
61 the Qingshi Lake Reservoir, which is one of the core areas of the Huixian karst wetland. The
62 geographical coordinates of the watershed are $110^{\circ} 09'$ to $110^{\circ} 14'$ east longitude and $25^{\circ} 04'$
63 to $25^{\circ} 08'$ north latitude, and the Mudong River Basin area is about 31.09 km^2 (Figure 1). The river
64 basin has a subtropical monsoon climate, with an average annual temperature of about 20°C and an
65 average annual precipitation of 1,800 mm, with uneven distribution of precipitation, with 75%-80%
66 of the precipitation concentrated in the rainy season from April to September.

67 The topography of the Mudong River basin is mainly characterized by undulating peaks and valleys
68 and basin plains, with isolated peaks scattered across the area. The northern part is mountainous,
69 while the southern part is relatively flat, showing an overall topographic pattern of higher elevation
70 in the north and lower in the south. The land use in the Mudong River basin is primarily agricultural,
71 with rice cultivation occupying a significant proportion of the total basin area. In addition, residential
72 areas, orchards, grasslands, and a small amount of water bodies are also distributed throughout the
73 basin.

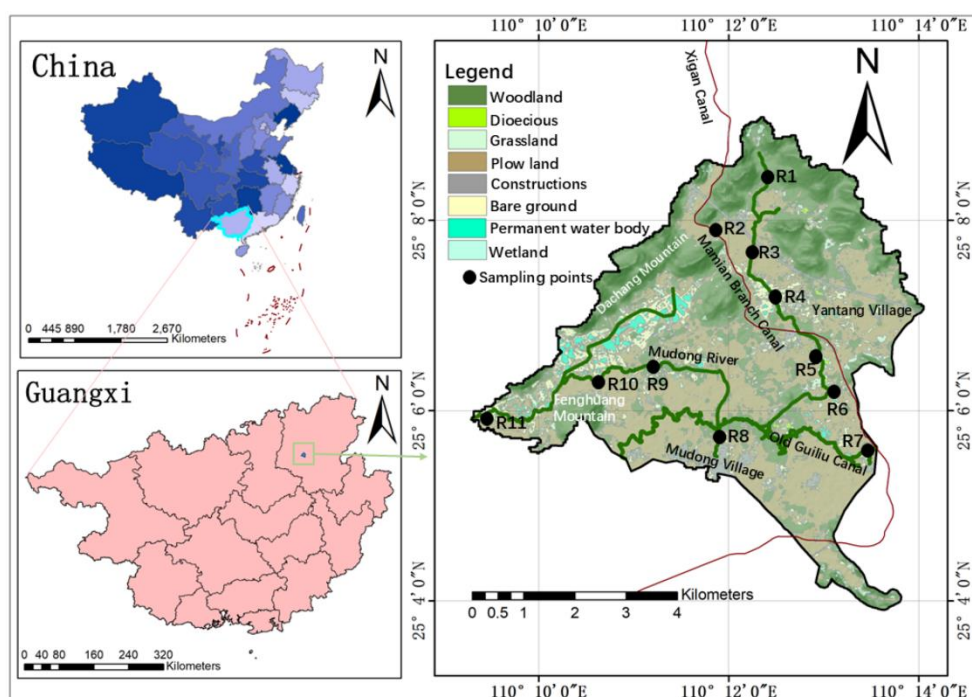


Figure 1. Location map of the study area

2.2 Sample collection and testing

Regarding the sampling and monitoring of N and P pollution concentrations, based on the representativeness of the point data and safety portability during sampling, a total of 11 sampling points in the study area were selected, and water samples from 10 of them (no R5 points) were chosen to be sent for testing of hydroxide isotopes and nitrogen and oxygen isotopes. The water samples were collected monthly from May 2020 to September 2024, a total of 28 times. Two groups of water samples were sent for hydroxide isotope and nitrate nitrogen, and oxygen isotope tests during the dry and rainy seasons from 2020 to 2021. The field sampling was operated according to the Technical Specification for Surface Water and Wastewater Monitoring (HJ/T91-2002) and combined with the actual situation on site. Table 1 shows the detection method of each index.

Table 1. Table of detection methods for various water quality parameters

Testing program	Detection methods	Main instruments used
TN	Alkaline potassium persulfate digestion UV spectrophotometric method (HJ636-2012)	UV-6000
NO ₃ ⁻ -N	Ultraviolet spectrophotometric method (HJ / T 346-2007)	UV-Vis spectrophotometer

NH ₄ ⁺ -N	Nessler's reagent colorimetric method (HJ535-2009)	
TP	Ammonium molybdate spectrophotometric method (GB11893-89)	
TDP	Ammonium molybdate spectrophotometric method (GB11893-89)	
δD-H ₂ O and δ ¹⁸ O-H ₂ O	Mass spectrometry	Picarro L1115-i Liquid water and water vapor isotope analyzer
δ ¹⁵ N-NO ₃ ⁻ and δ ¹⁸ O-NO ₃ ⁻	The denitrifying bacteria method	Delta V-plus Stable isotope mass spectrometer

2.3 Data processing

In this study, data from both field monitoring and laboratory experiments were preliminarily organized using Excel 2019. Spatial distribution maps and nitrate migration overview maps were generated using ArcGIS 10.2 and its 3D extension module, ArcScene. All other figures were created in Origin 2024. To quantitatively analyze nitrate pollution sources, this study employed surface water nitrate nitrogen and oxygen dual isotope data (δ¹⁵N-NO₃⁻ and δ¹⁸O-NO₃⁻). Within the R programming environment, the simmr package was utilized to construct Bayesian mixture models, estimating the contribution ratios of potential pollution sources during both dry and rainy seasons.

3 Results and analysis

3.1 Spatio-temporal characteristics of Nitrogen and Phosphorus and identification of driving factors

3.1.1 Spatial and temporal variation characteristics of Nitrogen and Phosphorus

During the monitoring period (2020–2024), the catchment-averaged annual precipitation was 2,604 mm, with the maximum annual total of 3,177 mm recorded in 2024 and the minimum of 2,084 mm in 2023. In accordance with long-term rainfall statistics and the fertilization–irrigation schedule of the dominant crop (rice), the hydrologic year is partitioned into a rainy season (April–September) and a dry season (October–March).

103 In the study area, the flow velocity of surface water ranged from 0 to 0.88 m/s during the dry season
104 and from 0 to 1.53 m/s during the rainy season. With the exception of site R8, the mean flow velocities
105 at all monitoring points were lower in the dry season than in the rainy season. Minimum flow
106 velocities were predominantly recorded in December, while maximum values generally occurred in
107 May, indicating strong seasonal variability. During the dry season, water temperature and dissolved
108 oxygen (DO) concentration fluctuated between 7.1°C and 33.6°C and 1.2 mg L⁻¹ and 44 mg L⁻¹,
109 respectively. In the rainy season, these parameters ranged from 15.2°C to 40.4°C and 0.3 mg L⁻¹ to
110 21.4 mg L⁻¹, showing a clear seasonal variation trend. In contrast, pH values were 5.67–8.74 in the
111 dry season and 6.51–8.52 in the rainy season, showing no significant seasonal effect. From June 2023
112 to September 2024, additional electrical conductivity (EC) measurements were taken across 11
113 sampling campaigns at the monitoring sections, comprising 2 campaigns in the dry season and 9 in
114 the rainy season. The EC values varied from 82.1 µS/cm to 461 µS/cm, with only site R2 exhibiting
115 a notably wider range of variation.

116 During the monitoring interval, both TN and NO₃⁻-N exhibited pronounced temporal variability. Dry-
117 season concentrations ranged from 0.111–9.496 mg L⁻¹ for TN and 0.014–6.691 mg L⁻¹ for NO₃⁻-N,
118 whereas rainy-season values spanned 0.023–7.047 mg L⁻¹ and 0.005–5.012 mg L⁻¹, respectively.

119 Owing to the high dispersion of NH₄⁺-N and TDP data, arithmetic means were deemed non-
120 representative; consequently, median values are reported to characterize the central tendency of these
121 solutes. Median NH₄⁺-N and TDP concentrations were 0.339 mg L⁻¹ and 0.028 mg L⁻¹ in the dry
122 season, and 0.360 mg L⁻¹ and 0.041 mg L⁻¹ during the rainy period.

123 In accordance with the Guilin Water Functional Area Planning and referencing the Environmental

124 Quality Standards for Surface Water (GB3838-2002) (Ministry of Environmental Protection of the
 125 People's Republic of China, 2002), the concentrations of N and P in the surface water of the Mudong
 126 River Basin generally comply with the Class III water quality standards (Table 2). During the
 127 monitoring period, 70.6% of the surface water samples exhibited TN concentrations exceeding 1.0
 128 mg/L. Notably, the exceedance rate for $\text{NH}_4^+\text{-N}$ was 12.0%, significantly higher than that for $\text{NO}_3^-\text{-N}$
 129 N, which showed no exceedance (0%). Additionally, 14.4% of samples had TP concentrations
 130 surpassing the 0.2 mg/L threshold. These results indicate that TN is the primary non-point source
 131 pollutant in the river basin.

132 **Table 2. Statistics on the exceedance rates of N and P pollution during the dry season and the rainy season**

Indicator	GB3838-2002III water standard	Dry season exceedance rate (%)	Rainy season exceedance rate (%)	Total exceedance rate (%)
TN	≤ 1.0	77.7	66.4	70.6
$\text{NO}_3^-\text{-N}$	≤ 10	0	0	0
$\text{NH}_4^+\text{-N}$	≤ 1.0	15.3	10.4	12.0
TP	≤ 0.2	10.4	16.5	14.4

133 During the dry season, the mean proportions of $\text{NO}_3^-\text{-N}$ and $\text{NH}_4^+\text{-N}$ in TN were 46.3% and 28.3%,
 134 respectively, while during the rainy season, these values were 44.2% and 31.6%, respectively (Figure
 135 2a). $\text{NO}_3^-\text{-N}$ constituted the dominant form of TN loss. The mean proportions of TDP in TP during
 136 the dry and rainy seasons were 49.8% and 47.5%, respectively (Figure 2b). TDP represented the
 137 predominant form of TP in surface river water, with no significant seasonal variation observed.

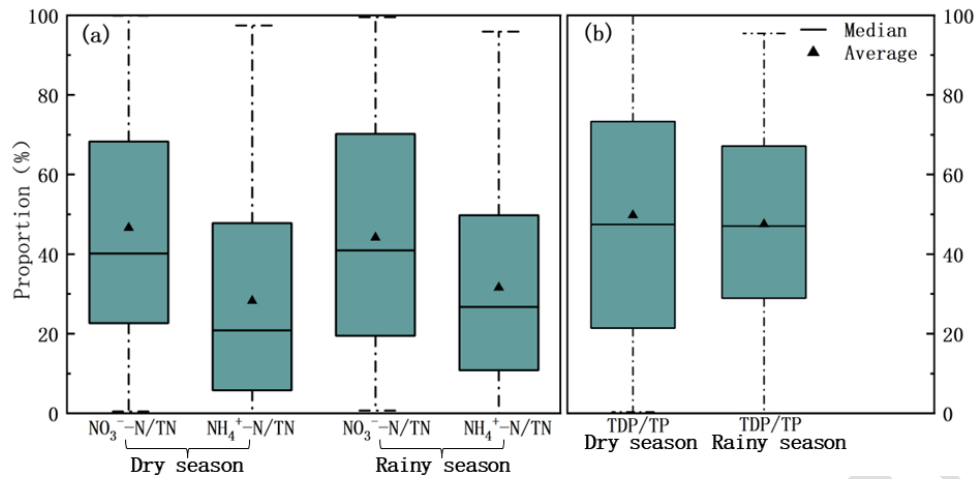


Figure 2. Ratios of $\text{NO}_3^- \text{-N/TN}$ (a), $\text{NH}_4^+ \text{-N/TN}$ (a), and TDP/TP (b) during the dry and rainy seasons

Based on the influences of precipitation, topography, karst development, and Quaternary sediment thickness, the study area was classified into three hydrodynamic zones (Pan et al., 2021): the northern recharge area (R1–R2), the central runoff area (R3–R8), and the western discharge area (R9–R11). As shown in Figure 3, the mean TN concentration in the northern recharge area ranged from 1.174 mg/L to 2.636 mg/L. The mean $\text{NO}_3^- \text{-N/TN}$ ratios at the two monitoring sites were 70.5% and 40.3%, respectively, which were higher than those at other sites. In the central runoff area, the mean TN concentration varied between 0.948 mg/L and 4.292 mg/L, with the mean $\text{NO}_3^- \text{-N/TN}$ ratio ranging from 24.6% to 69.4%. Among these, site R7 exhibited the lowest ratio. In the western discharge area, the mean TN concentration ranged from 1.329 mg/L to 3.839 mg/L, while the mean $\text{NO}_3^- \text{-N/TN}$ ratio varied between 28.9% and 38.4%. The mean TP concentration in the northern recharge area ranged from 0.029 mg/L to 0.045 mg/L. In the central runoff area, the mean TP concentration varied between 0.047 mg/L and 0.185 mg/L, with site R8 showing the highest value. In the western discharge area, the mean TP concentration ranged from 0.079 mg/L to 0.231 mg/L, exhibiting an increasing trend along the flow path and reaching its maximum at the outflow site R11.

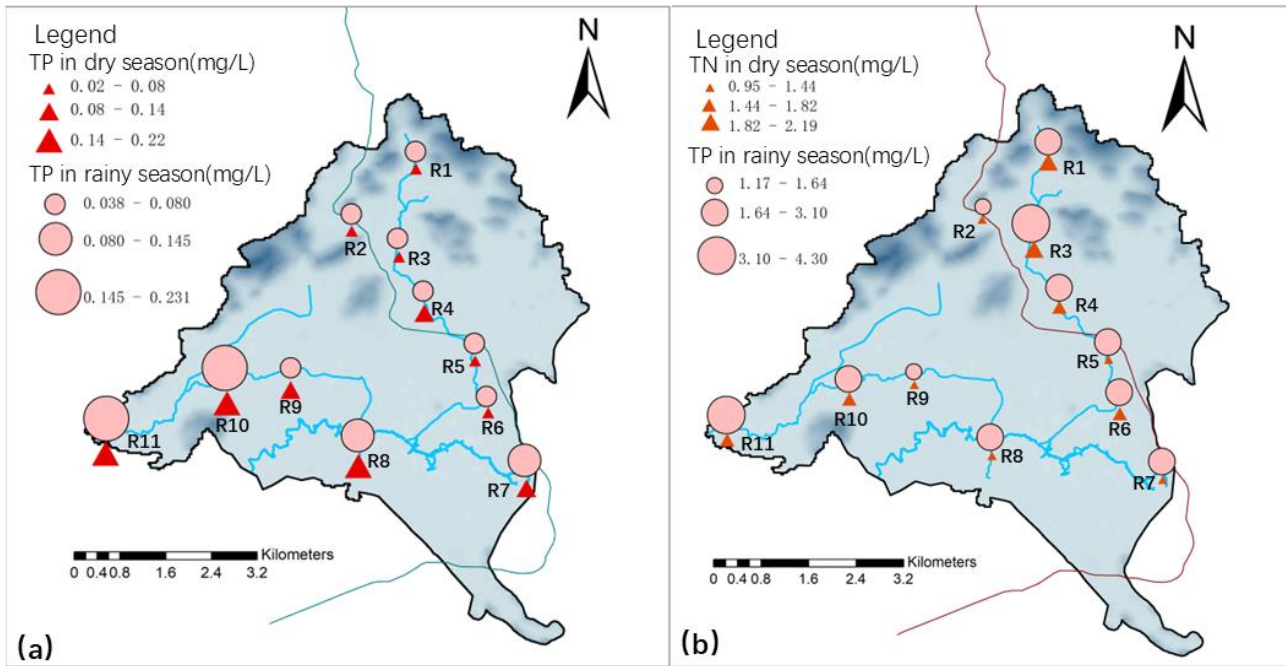


Figure 3. Spatial variation of TP (a) and TN (b) in surface water during the dry and rainy seasons

3.1.2 Statistical test for seasonal variation in water quality

To verify the statistical significance of differences between the dry and rainy seasons, this study employed the Mann-Whitney U test (also known as the Whitney-Wilcoxon test) for statistical analysis. Due to insufficient EC sample numbers, these were excluded from statistical parameters. The statistical measures included the test statistic U value, standardized Z value, and asymptotic significance P value, with the significance level set at $\alpha=0.05$ (Table 3).

Table 3. Results of the Mann-Whitney U test for seasonal differences in water quality parameters

Parameter	U Statistics	Z value	P-value	Significance ($\alpha=0.05$)	Median trend
Flow velocity	4763.5	-1.711	0.087	NO	No significant difference
Water temperature	1405.5	-15.316	<0.0001	YES	Dry<Rainy
pH	17109	1.792	0.073	NO	No significant difference
DO	17588.5	7.302	<0.0001	YES	Dry>Rainy
TN	21526.5	4.786	<0.0001	YES	Dry>Rainy
TP	15908.5	-0.865	0.387	NO	No significant difference

Calculation results indicate that significant seasonal differences ($p<0.0001$) exist in three parameters: water temperature, DO, and TN. The median water temperature during the rainy season is higher than

that in the dry season, directly reflecting significant seasonal temperature changes. In contrast, the DO concentration in the dry season is significantly higher than in the rainy season. This pattern can be attributed to two main factors: higher water temperatures directly limit oxygen solubility, while microbial activity during the rainy season accelerates oxygen consumption. In addition, abundant rainfall and runoff in the rainy season dilute nitrogen-containing pollutants, resulting in significantly higher total nitrogen concentrations in the dry season compared to the rainy season. Although the median total phosphorus concentration does not show obvious seasonal variation, its coefficient of variation reaches 110.94% in the dry season, compared to only 89.04% in the rainy season, indicating significant differences. This pattern is generally observed in nutrient parameters (Luo et al., 2024).

3.1.3 PCA: identifying driving factors

Based on monitoring and experimental data, this study used Principal Component Analysis (PCA) to explore the correlations among key water quality parameters. These parameters include flow velocity, water temperature, pH, dissolved oxygen (DO), total nitrogen (TN), and total phosphorus (TP). The eigenvalues of the first three principal components (PC1, PC2, and PC3) are all have eigenvalues greater than 1, collectively explaining 67.79% of the cumulative variance. To more fully reflect the variability of the data, PC4 is included as one of the main driving conditions for water quality changes, contributing to a cumulative variance of 82.03%.

Table 4. Results of the Principal Component Analysis (PCA)

Principal Component	Eigenvalue	Variance Percentage (%)	Cumulative Variance
PC1	1.692	28.21%	28.21%
PC2	1.253	20.89%	49.09%
PC3	1.133	18.88%	67.97%
PC4	0.843	14.05%	82.03%
PC5	0.693	11.55%	93.57%

PC6	0.386	6.43%	100.00%
-----	-------	-------	---------

Principal component (PC1) has high loadings on water temperature (0.647) and DO (-0.607), showing an inverse relationship between these two parameters. An increase in water temperature directly reduces the solubility of oxygen in water and accelerates microbial oxygen consumption. This shows that water temperature is a primary driver of water quality changes and indirectly reveals that water quality exhibits significant seasonal variation. PC2 is composed of nutrient factors TP (0.790) and TN (0.512), which are related to water eutrophication. The most probable causes are fertilization in orchards and farmland within the watershed and the discharge of domestic agricultural wastewater. PC3 and PC4 respectively show a positive correlation between flow velocity and pH value and a negative correlation. High-flow areas promote water re-oxygenation, reduce carbon dioxide concentration, and increase pH; conversely, low-flow areas, due to greater water stability, create a more suitable environment for plant growth. Photosynthesis consumes more carbon dioxide in the water, yet the pH continues to rise.

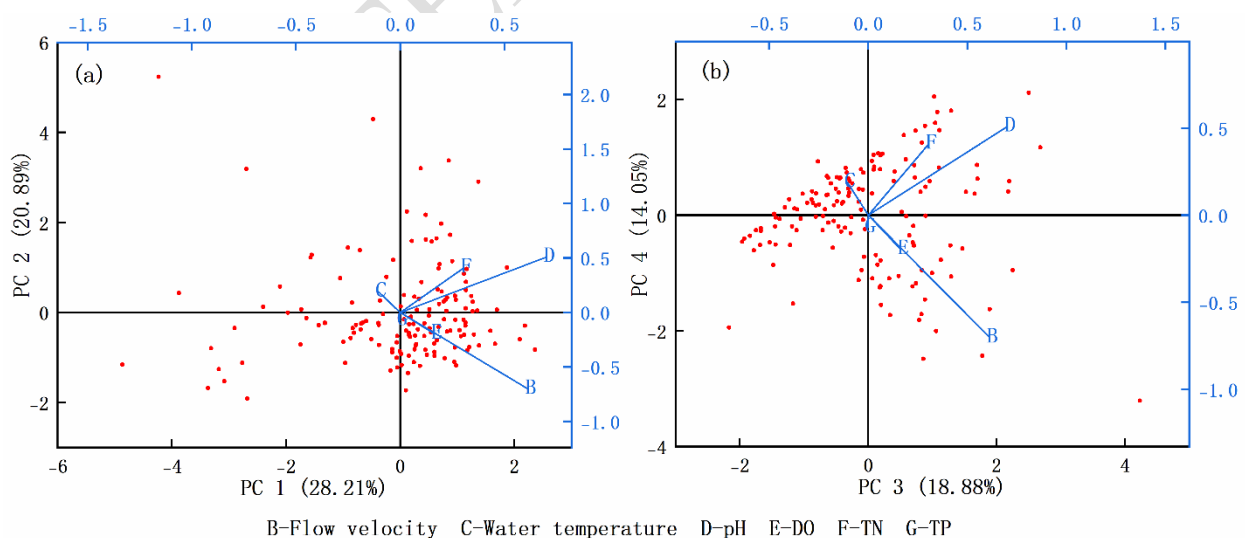


Figure 4. PCA Biplot: PC1 vs. PC2 (a), PC3 vs. PC4 (b)

194 3.2 Transport characteristics of Nitrogen and Phosphorus

195 3.2.1 Hydrogen and oxygen isotope signatures

196 During the dry season, the range of $\delta D-H_2O$ values in surface water was -35.98‰ to -22.97‰ and -
197 37.96‰ to -17.55‰, respectively. The range of $\delta^{18}O-H_2O$ values was -5.72‰ to -1.55‰ and -6.41‰
198 to -3.18‰, respectively.

199 Craig (1961) developed the global meteoric waterline (GLMWL) relationship equation:

$$200 \quad \delta D-H_2O = 8\delta^{18}O-H_2O + 10 \quad (1)$$

201 The local meteoric waterline (LMWL) equation for Guilin established by Wu et al. (2013) is:

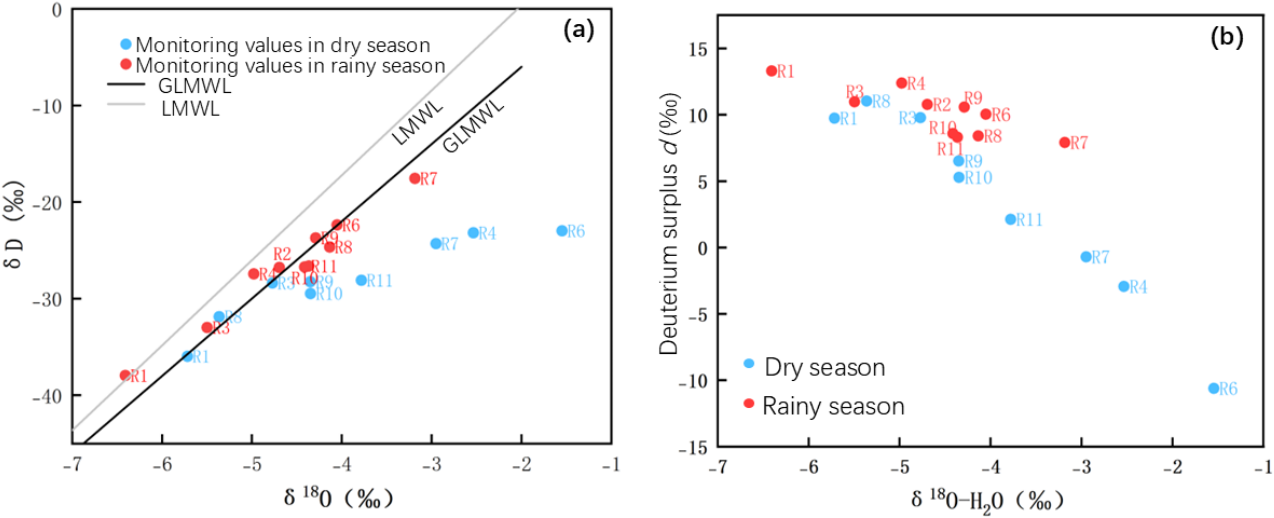
$$202 \quad \delta D-H_2O = 8.8\delta^{18}O-H_2O + 17.96 \quad (2)$$

203 Based on the LMWL and combined with the $\delta D-H_2O$ and $\delta^{18}O-H_2O$ hydrogen and oxygen isotope
204 values of surface water in the study area, the isotope points of both $\delta D-H_2O$ and $\delta^{18}O-H_2O$ are
205 distributed near the LMWL. This indicates that atmospheric precipitation is the primary source of
206 replenishment for surface water (Figure 5a).

207 The deuterium surplus d , first proposed by Dansgaard (1964), is an important isotopic parameter, and
208 it is believed that there is a correspondence between d values and local atmospheric precipitation
209 values. Based on this property, the source of recharge of water bodies can be effectively traced. During
210 the water cycle, the d value usually shows a decreasing trend with the enrichment of $\delta^{18}O-H_2O$
211 isotopes, and increases accordingly with the weakening of evaporation intensity. Therefore, the d -
212 value can be used as a preliminary indicator to determine the degree of isotope exchange and the
213 intensity of evaporation in water bodies.

214 During the dry and rainy seasons, surface water $\delta^{18}O$ values ranged from -10.61‰ to 11.04‰ and

215 7.91‰ to 13.30‰, respectively. Variations in $\delta^{18}\text{O}\text{-H}_2\text{O}$ values among sampling points resulted in
 216 corresponding changes in d values. As shown in Figure 5b, the lowest d values during the dry season
 217 were recorded at points R6 (-10.61‰) and R7 (7.91‰). This may be attributed to their location in the
 218 Mudong Lake of Huixian wetland, characterized by a large surface area, slow flow velocity, and high
 219 evaporation intensity. The highest $\delta^{18}\text{O}\text{-H}_2\text{O}$ value during the dry season was recorded at R8 (11.04‰),
 220 likely because water flow at this point is restricted, the surface is persistently covered by water
 221 hyacinth, and evaporation intensity is low.



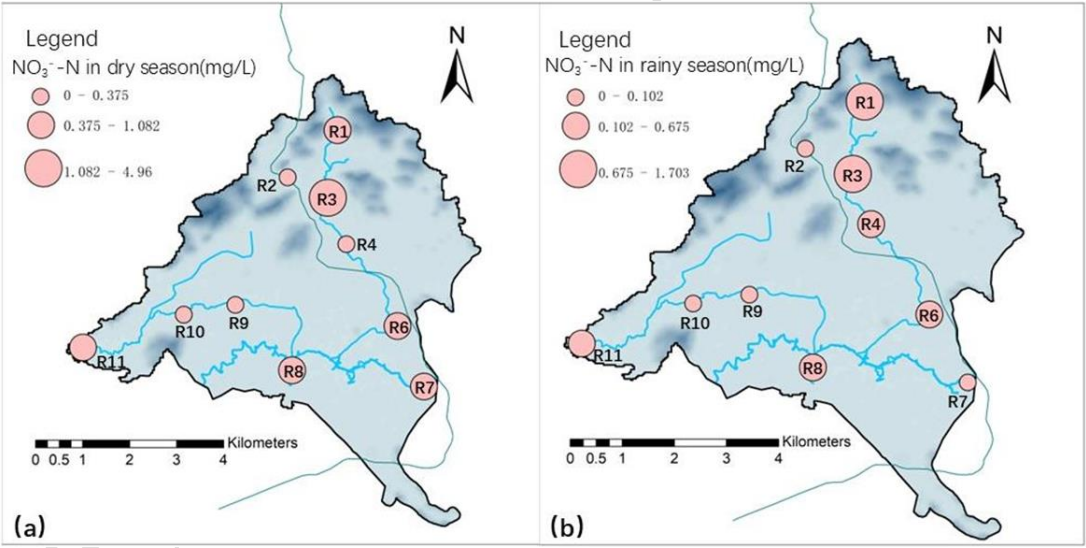
222 **Figure 5. Relationship between δD and $\delta^{18}\text{O}$ (a); d and $\delta^{18}\text{O}\text{-H}_2\text{O}$ (b) in surface water**

223 **3.2.2 Spatio-temporal distribution characteristics of nitrates**

224 Rainfall exerts a certain influence on nitrate concentrations (Carey et al., 2014; Husic et al., 2023).
 225 Based on the monthly precipitation data for the study area in 2020, the monitoring period was divided
 226 into the rainy season (May–September 2020) and the dry season (October–December 2020). During
 227 the dry season, nitrate concentrations ranged from 0.040 mg/L to 5.5 mg/L, showing an overall
 228 upward trend as months progressed. During the rainy season, nitrate concentrations ranged from
 229 0.009 mg/L to 3.731 mg/L. Over the course of the months, nitrate concentrations in the water

230 generally increased. The increase in June was slight, likely due to higher rainfall diluting nitrate
 231 concentrations in surface water.

232 Spatially (Figure 6), during the dry season, nitrate concentrations at all sampling points except R3
 233 and R11 averaged below 1 mg/L. Among these, R3 recorded the highest nitrate concentration, while
 234 R9 had the lowest. During the rainy season, nitrate concentrations at all sampling points except R1
 235 and R3 averaged below 1 mg/L. Point R1 recorded the highest average nitrate concentration, while
 236 Point R9 had the lowest. Throughout the monitoring period, nitrate concentrations in upstream
 237 Mudong River samples were generally high, whereas those in the middle and lower reaches of
 238 Mudong River and in the ancient Guiliu Canal were relatively low.

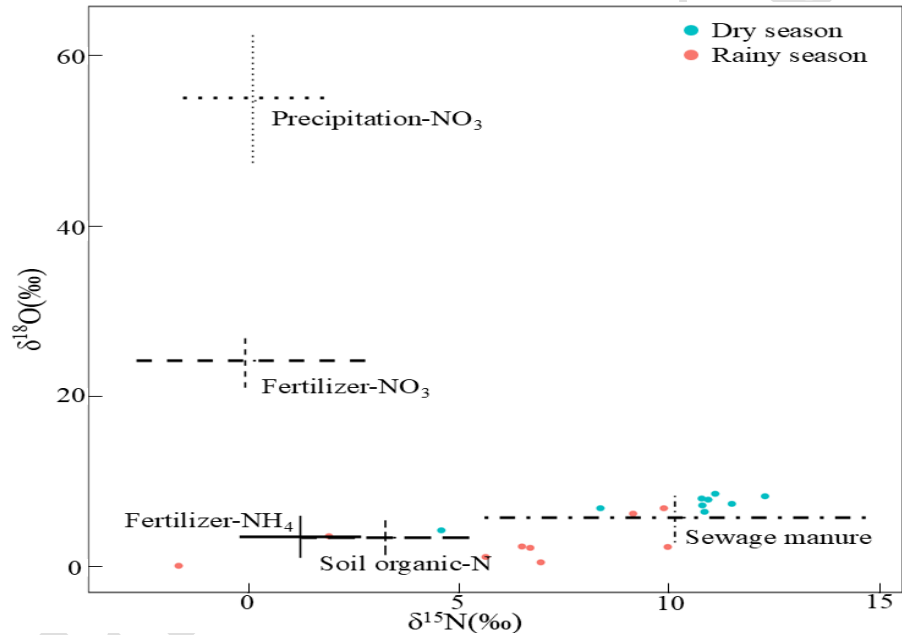


239 **Figure 6. Spatial distribution of nitrate concentration during the dry season (a) and the rainy season (b)**

240 **3.2.3 Quantitative contribution of pollutant sources based on Bayesian Mixture Models**

241 Based on $\delta^{15}\text{N-NO}_3^-$ and $\delta^{18}\text{O-NO}_3^-$ nitrogen-oxygen isotope data from surface water in the study
 242 area, the variation range of $\delta^{18}\text{O-NO}_3^-$ is 0.037‰ to 6.796‰, while that of $\delta^{15}\text{N-NO}_3^-$ ranges from
 243 1.651‰ to 9.969‰. Based on the characteristics of potential pollution sources in the study area (Li
 244 et al., 2022), five terminal pollution sources were established: precipitation-NO₃, fertilizer-NO₃,

245 fertilizer-NH₄, soil organic-N, and sewage manure. The model was run using a Markov Chain Monte
 246 Carlo simulation. Convergence diagnostics ($R\text{-hat} \approx 1.0$) confirmed the model's excellent stability.
 247 Figure 7 displays the distribution of various pollution sources and samples in the $\delta^{15}\text{N}$ – $\delta^{18}\text{O}$ dual
 248 isotope space. The figure reveals that sample points exhibit clustering trends across different seasons:
 249 dry-season samples cluster more toward the sewage manure region, while rainy-season samples shift
 250 distinctly toward the soil organic-N region. This preliminary finding indicates seasonal variations in
 251 pollution sources.



252 **Figure 7. Isotope spatial map**

253 According to the model output results (Table 5), during the dry season, sewage and manure are the
 254 main sources (37.9%), followed by soil organic-N (23.6%) and nitrate from precipitation (17.6%).
 255 However, in the rainy season, soil organic-N contributes the most (63.1%), far exceeding sewage and
 256 manure (13.9%) and nitrate from precipitation (10.4%).

Table 5. Comparison of contribution rates of pollution sources during the dry and rainy seasons (median %)

Pollution source	Dry season	Rainy season	Change quantity
Precipitation-NO ₃	17.6	10.4	-7.2
Fertilizer-NO ₃	3.4	4.8	+1.4
Fertilizer-NH ₄	2.2	3.0	+0.8
Soil organic-N	23.6	63.1	+39.5
Sewage manure	37.9	13.9	-24.0

As shown in Figure 8, the posterior distribution curves of soil organic-N and wastewater manure exhibit a clear separation between the dry and rainy seasons, with very little overlap. This indicates a significant difference in their contributions across different seasons.

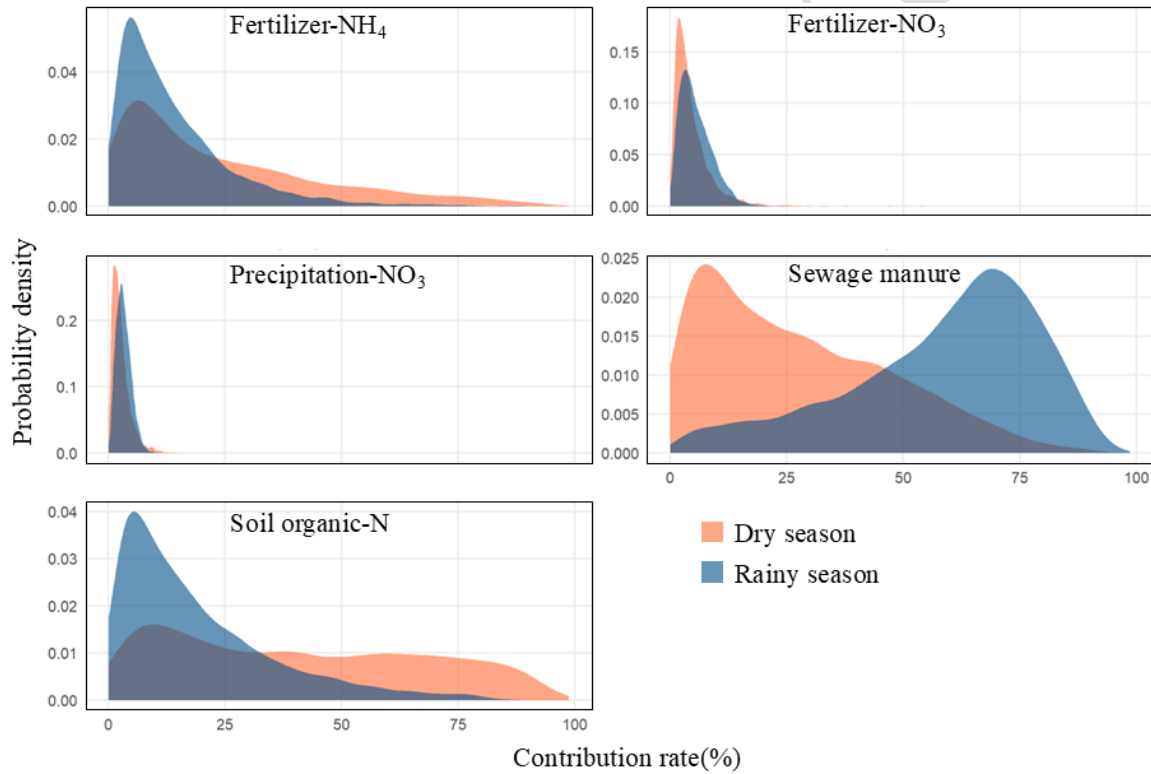


Figure 8. Posterior probability density distribution of pollution source contribution rate

4 Discussion

The velocity of flow of surface water in the study area was significantly high during the rainy season as compared to the dry season, which exhibit such typical seasonal pattern. Water temperatures were higher much during rainy seasons and concentrations of DO were lower. This was partly due to the

fact that raising the temperature of the water decreases the solubility of the oxygen molecule in water. Moreover, the rainfall during the rainy season increased organic matter input to the surface, which in turn increased the dissolved oxygen consumption (Zhang et al., 2024). Demars (2019) also reported this phenomenon.

According to the result of study that the total nitrogen (TN) concentration during dry season is far more compared to rainy season. The weakening of dilution caused by heavy rainfalls and runoff in the monsoon season is a plausible reason for loss of nitrogen retention capacity. In terms of TP, there are no significant differences between dry and wet seasons in total phosphorus (TP). However, in dry season, total phosphorus (TP) has a CV of 110.94 percent as compared to 89.04 percent in rainy season. The control of local inputs and outputs is related to this variation. According to earlier studies, the variations of total phosphorus in watersheds are usually tied with a heavy rainfall, runoff, and sediment resuspension (Zhang et al., 2022; Bender et al., 2018). The considerable variability of total phosphorus (TP) in the dry season during this study was related to domestic sewage and agricultural runoff.

Isotope values in water, or $\delta D-H_2O$ and $\delta^{18}O-H_2O$, are affected by soil type and vegetation cover at the point where atmospheric precipitation recharges surface rivers and shallow groundwater. As a result, these values vary seasonally and spatially. In the dry months, it is observed that lesser cooling, less rainfall and greater evaporation cause generally higher isotope values at various sampling sites. The Local meteoric waterline (LMWL) of Guilin is also further away from these values. The wet season that is hot, humid, and rainy consists of surface runoff, wetland seepage, and the replenishment of irrigation water. As a result, the abundance value of isotopes of hydrogen and oxygen tend to be

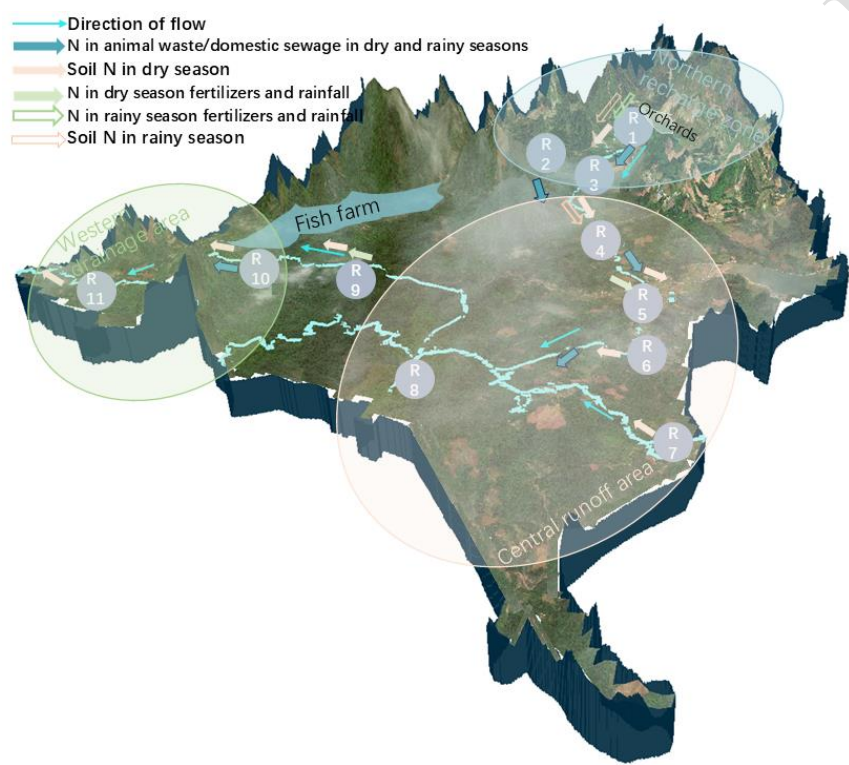
288 closer to the LMWL of Guilin.

289 R1 and R3 are both located next to orchards with R1 and vegetable fields with R3 which had high

290 average nitrate concentrations among other explanation including application of fertilizer. Water flow

291 velocity near R6 tends to be very low, which results in capturing animal dung and domestic sewage.

292 Thus, average nitrate concentration is high. Figure 9 shows the movement of nitrate in this watershed.



293 **Figure 9. Schematic diagram of NO_3^- transport in the surface water of the river basin**

294 Seasonal changes in pollution source contributions highlight the impact of surface conditions and

295 hydrological processes on nitrogen movement. There was a remarkable jump in the soil organic-N

296 from 23.6% in dry season to 63.1% in rainy season giving a total of 39.4%, which shows that the

297 leaching and eroding of nitrogen in the soil due to rainwater is the primary cause of nitrate pollution

298 during the rainy season. Throughout the dry season, sewage manure contributed approximately 37.9%

299 of total nitrogen in the rivers. This value decreased to 13.9% in the rainy season, showing a change

300 of -24.0%. This indicates that non-point source pollution gets diluted during the rainy season. The
301 fraction of precipitation-NO₃ was greater in the dry season (17.6%) than in the rainy season (10.4%).
302 This dry season higher fraction might be due to the accumulation with atmospheric particulate matters
303 deposition whereas the rainy season lower fraction may be due to the wet deposition dilution effect.
304 Research findings show that nitrogen and phosphorus pollution sources within the study area exhibit
305 seasonal migration characteristics. However, this paper argues that collaborative efforts across
306 different seasons remain key to mitigating pollution. Regardless of the time of year, the region must
307 strengthen sewage pipeline survey and construction supervision, while strictly regulating the
308 wastewater discharge behavior of livestock farmers. Efforts should be made to promote the use of
309 ecological pesticides within the basin to reduce the usage rate of chemical fertilizers and pesticides.
310 The government needs to guide farmers to reduce fertilizer application before heavy rainfall to
311 prevent nutrient loss. In response to the proliferation of water hyacinth and poor water flow at point
312 R8, local governments must regularly carry out cleaning and dredging to prevent algal outbreaks. The
313 agricultural department should guide villagers to implement crop rotation systems to improve soil
314 structure and reduce fixed nitrogen and phosphorus inputs. In an era of rapid technological
315 development, local governments should also rationally utilize technology to advance environmental
316 protection efforts. Nitrate isotope tracing technology and Bayesian models can be used as routine
317 monitoring tools to accurately locate new pollution hotspots through annual tracing analysis and
318 conduct post-treatment assessments.

319 **5 Conclusion**

320 This research witnessed nonpoint source pollution of nitrogen and phosphorus in Mudong River basin.

321 This study adopted a long-term monitoring approach involving water quality sampling, PCA and
322 isotopes. TN, TP, and other parameter data which has been collected were analyzed to reach the
323 following findings:

324 (1) Water environmental factors in the surface water repository exhibit distinct seasonal regularity,
325 with TN pollution being the most prominent. The water temperature, DO and TN during the dry
326 season were significantly different from that during the rainy season.

327 (2) There are generally three factors that account for water quality. These are environmental factors
328 of water (water temp and DO), nutrient factors (TN and TP), and hydrodynamic conditions (flow
329 velocity and pH). Of the water environmental factors PC1 has the greatest effect.

330 (3) Nitrate pollution sources vary fundamentally with the seasons. The isotope analysis of hydrogen
331 and oxygen indicates that replenishment in this basin is dominated by atmospheric precipitation.
332 Using dual-isotope tracking and the simulation of a Bayesian mixed model, researchers found that
333 the main source of pollution was sewage manure during the dry season (contribution rate of 37.9%),
334 while this resource turned into soil organic-N during the rainy season (contribution rate of 63.1%).
335 This shows that during the rainfall season, the leaching of soil nitrogen by rainfall runoff within the
336 basin is the primary cause of nitrogen pollution.

337 This study integrates the characterization of the spatiotemporal distribution of N and P concentrations
338 along with nitrogen-oxygen isotope analysis to clarify N and P pollution sources, migration routes,
339 the relationship with geological conditions. Based on the nitrate nitrogen and ortho phosphate
340 seasonal trends observed during raining and dry season and its value of nitrogen-oxygen isotopes at
341 the different sampling site in the region, it is shown that agricultural fertilizer, domestic sewage and

geological condition determine their pollution migration. This study aims to provide more environmentally friendly approaches for future local cultivation, fertilization, and management practices.

Acknowledgments: The field sampling and isotope analysis of this paper were supported by the “National Natural Science Foundation of China (Grant No. 52269010), Guangxi Natural Science Foundation for Young Scientists Program (Grant No. 2024GXNSFBA010429), Guangxi Key Research and Development Program Project (Grant No. Gui Ke AB25069138 and Gui Ke AB25069160), and the Basic Ability Enhancement Program for Young and Middle-aged Teachers in Guangxi Universities (Grant No. 2024KY0062), Guilin Major Special Program for Scientific Research and Technological Development (Grant No. 20230102-2)”.

REFERENCES:

- Bender, M. A., dos Santos, D. R., Tiecher, T., Minella, J. P. G., de Barros, C. A. P., & Ramon, R. (2018). Phosphorus dynamics during storm events in a subtropical rural catchment in southern Brazil. *Agriculture, Ecosystems & Environment*, 261, 93-102.
- Crain, A. S. (2010). Nutrients, Select Pesticides, and Suspended Sediment in the Karst Terrane of the Sinking Creek Basin, Kentucky, 2004-06 (No. 2010-5167). US Geological Survey.
- Craig, H. (1961). Isotopic variations in meteoric waters. *Science*, 133(3465), 1702-1703.
- Carey, R. O., Wollheim, W. M., Mulukutla, G. K., & Mineau, M. M. (2014). Characterizing storm-event nitrate fluxes in a fifth order suburbanizing watershed using in situ sensors. *Environmental Science & Technology*, 48(14), 7756-7765.
- Dansgaard, W. (1964). Stable isotopes in precipitation. *tellus*, 16(4), 436-468.
- Demars, B. O. (2019). Hydrological pulses and burning of dissolved organic carbon by stream respiration. *Limnology and Oceanography*, 64(1), 406-421.
- Gong, C. J., Han, J. L., Dai, J. F., Xia, R., Wan, Z. P., Zhang, S. P., & Xu, J. X. (2024). Vertical distribution patterns of nitrogen and phosphorus in soil solution: insights from a wetland trial site in the Li River Basin. *Water*, 16(13), 1830.
- Guo, W. J., Zhang, D., Zhang, W. S., Li, S., Pan, K., Jiang, H., & Zhang, Q. F. (2023). Anthropogenic impacts on the nitrate pollution in an urban river: Insights from a combination of natural-abundance and paired isotopes. *Journal of Environmental Management*, 333, 117458.

371 Heffernan, J. B., Albertin, A. R., Fork, M. L., Katz, B. G., & Cohen, M. J. (2012). Denitrification and inference of
 372 nitrogen sources in the karstic Floridan Aquifer. *Biogeosciences*, 9(5), 1671-1690.

373 Husic, A., Fox, J. F., Clare, E., Mahoney, T., & Zarnaghsh, A. (2023). Nitrate hysteresis as a tool for revealing storm-
 374 event dynamics and improving water quality model performance. *Water Resources Research*, 59(1),
 375 e2022WR033180.

376 Liang, L. Y., Qin, L. T., Peng, G. S., Zeng, H. H., Liu, Z., & Yang, J. W. (2021). Non-point source pollution and
 377 long-term effects of best management measures simulated in the Qifeng River Basin in the karst area of
 378 Southwest China. *Water Supply*, 21(1), 262-275.

379 Li, J., Zhu, D. N., Zhang, S., Yang, G. L., Zhao, Y., Zhou, C. S., Lin, Y. S., & Zou, S. Z. (2022). Application of the
 380 hydrochemistry, stable isotopes and MixSIAR model to identify nitrate sources and transformations in surface
 381 water and groundwater of an intensive agricultural karst wetland in Guilin, China. *Ecotoxicology and*
 382 *Environmental Safety*, 231, 113205.

383 Liao, H., Jiang, Z., Zhou, H., Qin, X., & Huang, Q. (2022). Isotope-based study on nitrate sources in a karst wetland
 384 water, Southwest China. *Water*, 14(10), 1533.

385 Luo, A. Q., Chen, H. H., Gao, X. F., Carvalho, L., Zhang, H. T., & Yang, J. (2024). The impact of rainfall events on
 386 dissolved oxygen concentrations in a subtropical urban reservoir. *Environmental Research*, 244, 117856.

387 Ministry of Environmental Protection of the People's Republic of China. (2002). *Environmental quality standards*
 388 *for surface water (GB 3838-2002)*. Beijing: China Environmental Science Press.

389 Pan, L. Y., Dai, J. F., Wu, Z. Q., Huang, L. L., Wan, Z. P., Han, J. L., & Li, Z. N. (2021). Spatial and temporal
 390 variations of nitrogen and phosphorus in surface water and groundwater of Mudong river watershed in Huixian
 391 Karst wetland, southwest China. *Sustainability*, 13(19), 10740.

392 Reimann, T., Geyer, T., Shoemaker, W. B., Liedl, R., & Sauter, M. (2011). Effects of dynamically variable saturation
 393 and matrix-conduit coupling of flow in karst aquifers. *Water Resources Research*, 47(11).

394 Smith, V. H., Tilman, G. D., & Nekola, J. C. (1999). Eutrophication: impacts of excess nutrient inputs on freshwater,
 395 marine, and terrestrial ecosystems. *Environmental Pollution*, 100(1-3), 179-196.

396 Song, X. W., Gao, Y., Green, S. M., Dungait, J. A., Peng, T., Quine, T. A., Xiong, B. L., Wen, X. F., & He, N. (2017).
 397 Nitrogen loss from karst area in China in recent 50 years: An in-situ simulated rainfall experiment's assessment.
 398 *Ecology and evolution*, 7(23), 10131-10142.

399 Vitousek, P. M., Mooney, H. A., Lubchenco, J., & Melillo, J. M. (1997). Human domination of Earth's ecosystems.
 400 *Science*, 277(5325), 494-499.

401 Wu, X., Zhu, X. Y., Zhang, M. L., Bai, X., & Zhang, B. Y. (2013). High-resolution record of stable isotopic
 402 composition in atmospheric precipitation: A case study from Guilin area [in Chinese]. *Resources and*
 403 *Environment in the Yangtze Basin*, 22(2), 182-188.

404 Xue, D. M., Botte, J., De Baets, B., Accoe, F., Nestler, A., Taylor, P., Van Cleemput, O., Berglund, M., & Boeckx,
 405 P. (2009). Present limitations and future prospects of stable isotope methods for nitrate source identification in
 406 surface-and groundwater. *Water Research*, 43(5), 1159-1170.

407 Xu, R. H., Cai, Y. P., Wang, X., Li, C. H., Liu, Q., & Yang, Z. F. (2020). Agricultural nitrogen flow in a reservoir
 408 watershed and its implications for water pollution mitigation. *Journal of Cleaner Production*, 267, 122034.

409 Zhang, T., Zhou, L., Zhou, Y. Q., Zhang, Y. L., Guo, J. X., Han, Y. C., Zhang, Y. Y., Hu, L., Jang, K.-S., Spencer, R.
 410 G. M., Brookes, J. D., Dolfing, J., & Jeppesen, E. (2024). Terrestrial dissolved organic matter inputs

411 accompanied by dissolved oxygen depletion and declining pH exacerbate CO₂ emissions from a major Chinese
412 reservoir. *Water Research*, 251, 121155.

413 Zhang, M. Z., Krom, M. D., Lin, J. J., Cheng, P., & Chen, N. W. (2022). Effects of a storm on the transformation
414 and export of phosphorus through a subtropical river-turbid estuary continuum revealed by continuous
415 observation. *Journal of Geophysical Research: Biogeosciences*, 127(8), e2022JG006786.

ACCEPTED MANUSCRIPT